

SDSS-IV MaNGA:

The effect of stellar mass and halo mass on the assembly histories of satellite galaxies

GRECCO A. OYARZÚN,^{1,2} KEVIN BUNDY,³ KYLE B. WESTFALL,³ IVAN LACERNA,^{4,5} RENBIN YAN,^{6,7} J. R. BROWNSTEIN,⁸
NIV DRORY,⁹ AND RICHARD R. LANE¹⁰

¹*Astronomy Department, University of California, Santa Cruz, CA 95064, USA*

²*The William H. Miller III Department of Physics & Astronomy, Johns Hopkins University, Baltimore, MD 21218, USA*

³*University of California Observatories - Lick Observatory, University of California, Santa Cruz, CA 95064, USA*

⁴*Instituto de Astronomía y Ciencias Planetarias, Universidad de Atacama, Copayapu 485, Copiapó, Chile*

⁵*Millennium Institute of Astrophysics, Nuncio Monsenor Sotero Sanz 100, Of. 104, Providencia, Santiago, Chile*

⁶*Department of Physics, The Chinese University of Hong Kong, Shatin, N.T., Hong Kong SAR, China*

⁷*Department of Physics and Astronomy, University of Kentucky, 505 Rose St., Lexington, KY 40506-0055, USA*

⁸*Department of Physics and Astronomy, University of Utah, 115 S. 1400 E., Salt Lake City, UT 84112, USA*

⁹*McDonald Observatory, The University of Texas at Austin, 1 University Station, Austin, TX 78712, USA*

¹⁰*Centro de Investigación en Astronomía, Universidad Bernardo O Higgins, Avenida Viel 1497, Santiago, Chile*

(Accepted February 12, 2023)

ABSTRACT

We combine an unprecedented MaNGA sample of over 3,000 passive galaxies in the stellar mass range $10^9 - 10^{12} M_{\odot}$ with the Sloan Digital Sky Survey group catalog by Tinker to quantify how central and satellite formation, quantified by radial profiles in stellar age, [Fe/H], and [Mg/Fe], depends on the stellar mass of the galaxy (M_*) and the mass of the host halo (M_h). After controlling for M_* and M_h , the stacked spectra of centrals and satellites beyond the effective radius (r_e) show small, yet significant differences in multiple spectral features at the 1% level. According to spectral fitting with the code `alf`, a primary driver of these differences appears to be [Mg/Fe] variations, suggesting that stellar populations in the outskirts of satellites formed more rapidly than the outer populations of centrals. To probe the physical mechanisms that may be responsible for this signal, we examined how satellite stellar populations depend on M_h . We find that satellites in high- M_h halos show older stellar ages, lower [Fe/H], and higher [Mg/Fe] compared to satellites in low- M_h halos, especially for $M_* = 10^{9.5} - 10^{10.5} M_{\odot}$. These signals lend support to environmentally driven processes that quench satellite galaxies, although variations in the merger histories of central and satellite galaxies also emerge as a viable explanation.

Keywords: Early-type galaxies (429); Elliptical galaxies (456); Galaxies (573); Galaxy ages (576); Galaxy evolution (594); Galaxy stellar content (621); Quenched galaxies (2016); Galaxy abundances (574); Galaxy dark matter halos (1880); Galaxy environments (2029); Galaxy properties (615); Galaxy spectroscopy (2171)

1. INTRODUCTION

Evolution of structure in the Λ CDM model is hierarchical (White & Rees 1978; Davis et al. 1985). Massive central galaxies are thought to grow in stellar mass (M_*) and size through the accretion of stellar envelopes

from satellite galaxies (Oser et al. 2010; Johansson et al. 2012; Oser et al. 2012). Several observations have found supporting evidence for this picture. Cluster galaxies show an excess in surface brightness that can extend out to 100 kpc and beyond (intra-cluster light; Zibetti et al. 2005). Similarly, the surface brightness profiles of massive elliptical galaxies ($M_* > 10^{11} M_{\odot}$) contain faint, extended components at large radii ($r > 10$ kpc; Huang et al. 2013a,b) presumably accreted from satellite

galaxies (Huang et al. 2018). Furthermore, in Oyarzún et al. (2019) we showed that the stellar metallicity profiles of $M_* > 10^{11} M_\odot$ early-type galaxies (ETGs) flatten beyond the effective radius (r_e), which is another signature of stellar accretion (Cook et al. 2016; Taylor & Kobayashi 2017).

The hierarchical formation scenario can also successfully explain some of the differences between the central and satellite galaxy populations. At fixed M_* , satellite galaxies show higher stellar concentrations, older stellar populations, higher stellar metallicities, and a higher quenched fraction than central galaxies (van den Bosch et al. 2008a; Pasquali et al. 2010; Wetzel et al. 2012; La Barbera et al. 2014; Davies et al. 2019; Pasquali et al. 2019; Gallazzi et al. 2020; Trussler et al. 2021). These observations suggest that parent halos facilitate satellite quenching through mechanisms that can, for example, remove the subhalo ISM (i.e. ram-pressure stripping; Gunn & Gott 1972; Einasto et al. 1974; Nulsen 1982) or inhibit further star formation through the shutdown of cold gas accretion (e.g. starvation; Kawata & Mulchaey 2008).

At the low- M_* end ($M_* < 10^8 M_\odot$), ram-pressure stripping is thought to dominate satellite quenching (Weisz et al. 2015; Davies et al. 2016). Low- M_* satellites interact with the intra-cluster medium (ICM) of the parent halo, stripping their gas reservoirs and truncating their star-formation (e.g. Balogh & Morris 2000; Mayer et al. 2001, 2006; van den Bosch et al. 2008b; Spindler & Wake 2017). As a result, satellite galaxies show older stellar populations than centrals of the same M_* (Pasquali et al. 2010). At the same time, low- M_* satellites can lose some of their M_* through tidal stripping (Kang & van den Bosch 2008). As this process leaves stellar metallicity roughly unaltered (Pasquali 2015), low M_* satellites deviate from the average stellar mass-metallicity relation followed by central galaxies (Faber & Jackson 1976; Cid Fernandes et al. 2005; Gallazzi et al. 2005; Thomas et al. 2005, 2010; González Delgado et al. 2014; Pasquali 2015).

The impact of ram-pressure stripping is believed to decrease toward higher stellar masses ($M_* = 10^8 - 10^{11} M_\odot$), as deeper potentials can more effectively sustain drag from the ICM (Fillingham et al. 2015). At these masses, mechanisms that inhibit future star formation through environmental preprocessing are more likely to dominate. In starvation, satellite galaxies can lose their cold gas reservoirs through tidal interactions with the parent halo, suppressing future star-formation (Kawata & Mulchaey 2008). This process can also apply to hot subhalo gas in a process known as strangulation (e.g. Larson et al. 1980). These two mechanisms are thought

to act in timescales of 2-6 Gyr, after which the satellite galaxy quenches within 1 Gyr (*delayed-then-rapid*; Wetzel et al. 2012, 2013).

All of these mechanisms point to a strong connection between the satellite infall time (T_{inf}) and the satellite quenching time (T_q). To test this connection, Pasquali et al. (2019) and Smith et al. (2019) parameterized T_{inf} in projected phase space (distance and velocity of the satellite within the parent halo). Using this parameterization, Gallazzi et al. (2020) found ancient infallers ($T_{inf} > 5$ Gyr) to host older stellar populations and show higher stellar metallicities than recent infallers ($T_{inf} < 2$ Gyr). This result led Gallazzi et al. (2020) to conclude that ancient infallers likely quench through starvation and strangulation ($T_q > T_{inf}$). On the other hand, recent infallers probably quenched through internal processes, long before they entered the virial radius of the parent halo ($T_q < T_{inf}$).

Although this picture appears compelling, the true origin of some of the observational differences between centrals and satellites has been questioned. Wang et al. (2018b) showed that the quenched fraction, star-formation rates, and 4000Å breaks of centrals and satellites in the Sloan Digital Sky Survey (SDSS) are indistinguishable after both stellar mass and halo mass are controlled for. Similar results were later found for other galaxy properties like size and bulge-to-total light ratio (Wang et al. 2020). The similarities between the scaling relations followed by centrals and satellites could indicate that their quenching processes are not as different as initially thought (Wang et al. 2018c).

At this juncture, discerning whether satellite galaxies are subject to unique environment-driven processes can greatly benefit from spatially resolved spectroscopy. For instance, characterization of the stellar mass surface density profiles of satellites can reveal evidence of tidal stripping beyond the tidal radius (Read et al. 2006). Alternatively, modeling of the star-formation histories of satellite outskirts could reveal signatures of starvation or gas stripping (e.g. Cortese et al. 2021). These arguments have motivated several works to search for differences between the stellar population gradients of central and satellite galaxies. So far, all analyses with the MaNGA (Bundy et al. 2015) and SAMI (Allen et al. 2015) surveys have found no significant differences between the stellar age, metallicity, and $[\alpha/\text{Fe}]$ gradients of central and satellite galaxies (Goddard et al. 2017a; Zheng et al. 2017; Santucci et al. 2020).

The more direct interpretation of these results is that central and satellites quench in a similar fashion, in alignment with the interpretation by Wang et al. (2018b,c) and in contrast with the *delayed-then-rapid*

scenario. Alternatively, differences between the spatially resolved stellar populations of centrals and satellites could also be very subtle, requiring larger samples to isolate any signatures. For instance, [Greene et al. \(2015\)](#) were unable to compare the stellar population profiles of central and satellite galaxies at fixed M_* due to the size of the MASSIVE sample (~ 100 galaxies). Less than 1,000 galaxies had been observed by MaNGA at the time that [Goddard et al. \(2017a\)](#) and [Zheng et al. \(2017\)](#) performed their work on the stellar population gradients. This number is in strong contrast to the SDSS samples used by [Pasquali et al. \(2010\)](#); [Gallazzi et al. \(2020\)](#); [Trussler et al. \(2021\)](#), which exceeded 500,000 galaxies. However, now that the MaNGA survey is complete, in this paper we take advantage of the full sample that exceeds 10,000 galaxies. Taking into account signal to noise and the number of spectra per galaxy, the constraining power of MaNGA is now almost a factor of 2 larger than that of the SDSS MAIN Galaxy Survey Sample ([York et al. 2000](#); [Gunn et al. 2006](#); [Alam et al. 2015](#); [Oyarzún et al. 2022](#)).

Another possible source of uncertainty comes from stellar population characterization. Most fitting codes do not fit for individual element abundances, adding uncertainties to reported ages and metallicities ([Conroy 2013](#)). This is particularly relevant in light of variations in the abundance pattern of passive galaxies with the local environment (e.g. [Greene et al. 2019](#); [Oyarzún et al. 2022](#)). To account for these variations, in this work we use the stellar population fitting code `alf` ([Conroy & van Dokkum 2012](#); [Conroy et al. 2018](#)). This program is designed to capture uncertainties in stellar evolution, allowing us to fit for the age, abundance of various elements, and initial mass function (IMF) of stellar systems older than 1 Gyr.

The use of stellar population gradients in spatially resolved surveys adds to the difficulties. Linear fits to the stellar population profiles of ETGs can *wash out* underlying trends in the data ([Oyarzún et al. 2019](#)). For example, [Greene et al. \(2015\)](#) were only able to conclude that the ages of ETGs correlate with group richness by directly analyzing the stellar age profiles and their dependence on galaxy number density. In this paper, we overcome the limitations posed by the use of gradients by comparing the full extent of the stellar population profiles of central and satellite galaxies.

Cross contamination of central and satellite galaxy samples also presents a challenge. Group catalogs can sometimes struggle to reproduce the fractions of red and blue satellites, biasing the samples ([Tinker 2020a](#)). To mitigate this effect, we employ the SDSS group catalog by [Tinker \(2020b\)](#), which is calibrated on observa-

tions of color-dependent galaxy clustering and estimates of the total satellite luminosity to accurately reproduce the fraction of red and blue satellites for $M_* > 10^{11} M_\odot$. Furthermore, the [Tinker \(2020b\)](#) group catalog exploits deep photometry from the DESI Legacy Imaging Survey ([Dey et al. 2019](#)), allowing for the precise measurements of group luminosity required to estimate M_h .

This paper is structured as follows. In Section 2 we define our sample of passive central and satellite galaxies from SDSS-IV MaNGA. In Section 3, we describe our handling of the spectra and fitting with `alf`. We show our results in Section 4 and discuss the implications in Section 5. We summarize in Section 6. This work adopts a Kroupa IMF ([Kroupa 2001](#)) for estimating stellar masses. We assume $H_0 = 70 \text{ km s}^{-1} \text{ Mpc}^{-1}$, and all magnitudes are reported in the AB system ([Oke & Gunn 1983](#)).

2. DATASET

2.1. The MaNGA survey

The MaNGA survey ([Bundy et al. 2015](#); [Yan et al. 2016a](#)) was part of SDSS-IV ([York et al. 2000](#); [Gunn et al. 2006](#); [Blanton et al. 2017](#); [Aguado et al. 2019](#)) and provided spatially resolved spectroscopy for over 10,000 nearby ($z < 0.15$) galaxies ([Drory et al. 2015](#); [Law et al. 2015](#)). The spectra have a median spectral resolution of $\sigma = 72 \text{ km s}^{-1}$ ($R \sim 2,000$) and cover the wavelength range 3,600-10,300 Å ([Smee et al. 2013](#)). The data cubes typically reach a 10σ continuum surface brightness of $23.5 \text{ mag arcsec}^{-2}$, and their astrometry is measured to be accurate to $0''.1$ ([Law et al. 2016](#)). Radial coverage reaches between 1.5 and 2.5 r_e for most targets ([Wake et al. 2017](#)).

The data was reduced by the MaNGA Data Reduction Pipeline (DRP; [Yan et al. 2016b](#); [Law et al. 2016](#)). De-projected distances, stellar kinematic maps, and emission line fluxes were computed by the MaNGA Data Analysis Pipeline (DAP; [Belfiore et al. 2019](#); [Westfall et al. 2019](#)). Effective radii (r_e) for all MaNGA galaxies were retrieved from the NASA-Sloan Atlas¹ (NSA). These r_e were determined using an elliptical Petrosian analysis of the r -band image from the NSA, implementing the detection and deblending technique described in [Blanton et al. \(2011\)](#). For data access and handling, we used the tool `Marvin`² ([Cherinka et al. 2019](#)).

¹ <http://nsatlas.org>

² <https://www.sdss.org/dr17/manga/marvin/>

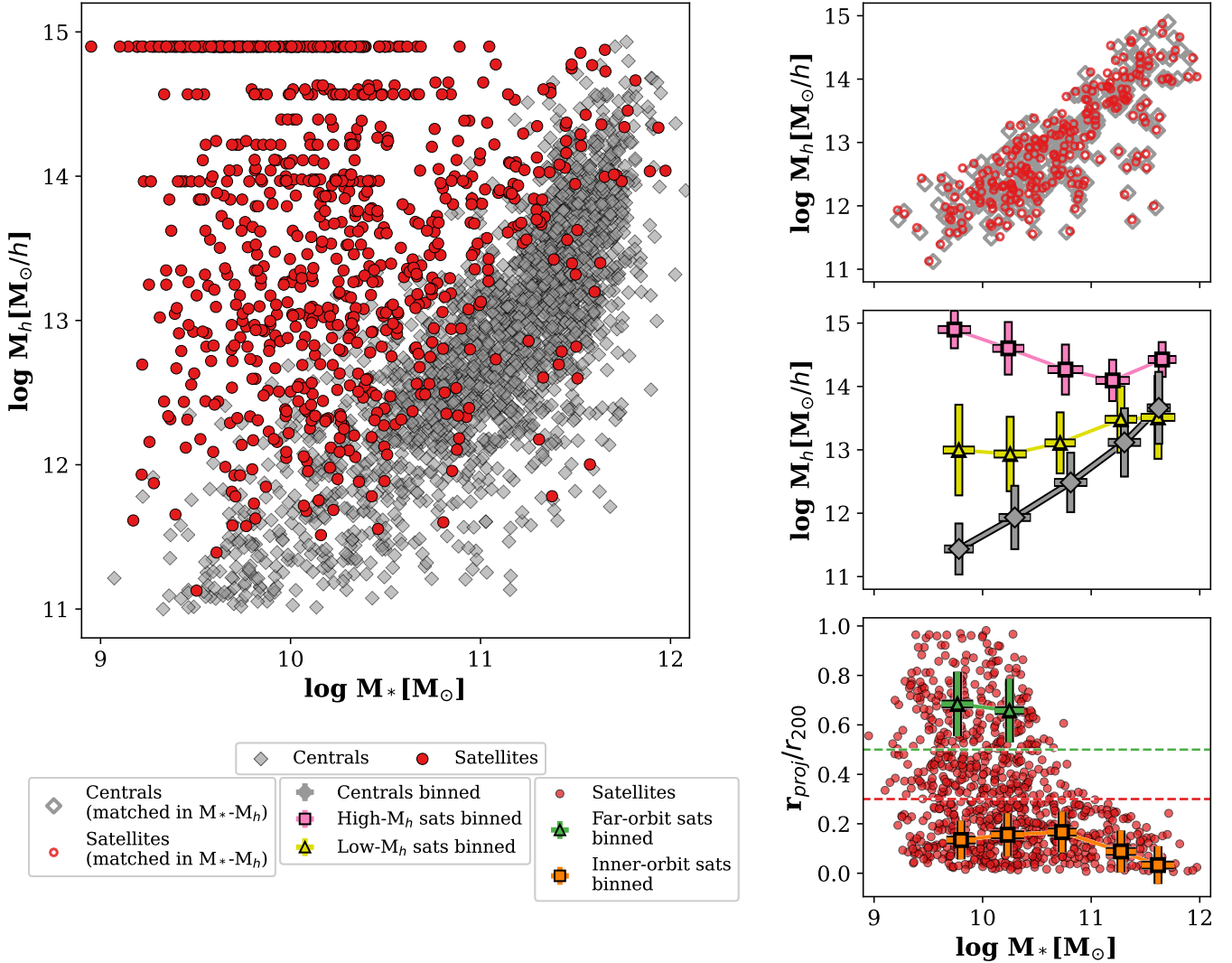


Figure 1. Distribution of passive MaNGA galaxies in stellar mass, halo mass, and normalized cluster-centric distance. Central/satellite classification and halo mass estimates come from the [Tinker \(2020b\)](#) catalog. Left: stellar-to-halo mass relation for centrals (gray) and satellites (red). On the right-hand side, the different panels show the different galaxy subsamples adopted in our analysis. Top right: central (gray) and satellite (red) subsamples with matching M_* and M_h . Middle right: central and satellite subsamples selected according to host halo mass. The average M_* and M_h of high- M_h and low- M_h satellites are shown as magenta squares and yellow triangles, respectively. The error bars show the standard deviation around the average values. Bottom right: satellite subsamples selected on normalized cluster-centric distance. The M_* and cluster-centric distances of inner-orbit satellites and far-orbit satellites are plotted in orange and green, respectively.

2.2. Sample

This work uses the final internal release of MaNGA data, known as MaNGA Product Launch 11 (MPL-11). The total number of galaxies in MPL-11 is 10,086. The approach to stellar population characterization that we implement in this paper is designed for old stellar systems only. Therefore, we removed star-forming systems by setting the criterion $\log(\text{sSFR}) < -11.5 M_\odot \text{yr}^{-1}$, where sSFR stands for spatially integrated specific star-formation rates measured in MaNGA as part of the

pipeline for the Pipe3D Value Added Catalog for DR17³ ([Sánchez et al. 2016a, 2022](#)) for Data Release 17 ([Abdurro'uf et al. 2022](#)). Since these sSFRs were corrected for dust attenuation using the Balmer decrement ([Sánchez et al. 2016b](#)), this method of estimating the intrinsic sSFR of galaxies is among the most reliable at low redshift (e.g. [Moustakas et al. 2006](#)). This selection resulted in a sample of 3957 passive galaxies, of

³ <https://www.sdss.org/dr17/manga/manga-data/manga-pipe3d-value-added-catalog/>.

Table 1. Number of galaxies in each subsample as a function of M_* ^a

	$M(M_\odot) = 10^{9.5} - 10^{10}$	$10^{10} - 10^{10.5}$	$10^{10.5} - 10^{11}$	$10^{11} - 10^{11.5}$	$10^{11.5} - 10^{12}$	Out of Range	Total
Centrals	111	211	514	948	412	21	2217
Satellites	273	319	133	67	25	85	902
Cens. (M_* - M_h matched)	27	69	64	54	23	4	241
Sats. (M_* - M_h matched)	27	70	63	54	23	4	241
Low- M_h sats.	132	154	88	26	12	38	450
High- M_h sats.	141	165	45	41	13	47	452
Inner-orbit sats.	112	160	109	67	25	31	504
Far-orbit sats.	90	90	5	0	0	35	220
Low- M_h inner sats.	61	75	71	26	12	14	259
High- M_h inner sats.	51	85	38	41	13	17	245
Low- M_h far sats.	46	45	4	0	0	20	115
High- M_h far sats.	44	45	1	0	0	15	105

^aNote that not all satellite galaxies are classified as either inner orbit or far orbit (bottom right panel of Figure 1).

which 2217 have more than a 90% probability of being a central and 902 have more than a 90% probability of being a satellite according to the Tinker (2020b) catalog (further details in Section 2.4).

2.3. Stellar masses

To estimate the stellar mass (M_*) of every galaxy, we first co-added the spectra within the r_e . Then, the mass within the r_e was measured by running the stellar population fitting code *Prospector*⁴(Leja et al. 2017) on the co-added spectrum.

Prospector samples the posterior distribution for a variety of stellar population parameters and star formation history (SFH) prescriptions. Stellar population synthesis is handled by the code FSPS⁵(Conroy et al. 2009; Conroy & Gunn 2010). Our runs adopted the MILES stellar library (Sánchez-Blázquez et al. 2006), MIST isochrones (Choi et al. 2016; Dotter 2016), and a Kroupa 2001 IMF. For the SFH, we implemented a nonparametric prescription with a continuity prior, emphasizing smooth SFHs over time (Leja et al. 2019).

The total stellar mass of the galaxy is then

$$M_*^{total} = 2M_*^{r_e} \times 10^{-0.15}, \quad (1)$$

where $M_*^{r_e}$ is the spectroscopic stellar mass within the effective radius. We measure an offset of 0.15 dex between our $2M_*^{r_e}$ and the stellar masses measured through k -correction fits to the Sersic fluxes in the NSA (Blanton

& Roweis 2007). This is not unexpected, since half-mass radii are smaller than half-light radii (García-Benito et al. 2017). We correct for this offset by multiplying our stellar masses by $10^{-0.15}$ (see the equation). In the rest of the paper, we will simply refer to M_*^{total} as M_* .

2.4. Local environment

This paper uses the Tinker (2020b) group catalog for the characterization of the local environment. This catalog is the implementation on SDSS of the self-calibrating halo-based galaxy group finder (Tinker 2020a). In the finder algorithm, the probability of a galaxy being a satellite is dependent on both galaxy color and luminosity. This allows Tinker (2020b) to accurately reproduce the fraction of massive quenched satellite galaxies and estimate M_h more accurately (Campbell et al. 2015). The Tinker (2020b) catalog also took advantage of deep photometry from the DESI Legacy Imaging Survey (Dey et al. 2019), allowing for precise group and galaxy M_* measurements. These improvements are key to accurately constraining M_h (Bernardi et al. 2013; Wechsler & Tinker 2018).

Yet, the approach in Tinker (2020a) still has its limitations. Like most group catalogs, it is susceptible to central galaxy misidentification. It also assumes that the total satellite luminosity is a function of halo mass only. The Tinker (2020b) catalog also fails to reproduce the clustering of faint quiescent galaxies ($M_* < 10^{9.5} M_\odot$). We minimize the impact of these biases by setting strict central and satellite identification criteria (next paragraph) and by avoiding the lowest M_* end of the galaxy population (our galaxies have $M_* > 10^9 M_\odot$; Figure 1).

⁴ *Prospector*

<https://github.com/bd-j/prospector/blob/master/doc/index.rst>

⁵ FSPS: Flexible Stellar Population Synthesis

<https://github.com/cconroy20/fps>

This work used the public version of the [Tinker \(2020b\)](#) group catalog⁶. Satellite probabilities (P_{sat}) were used to define central and satellite galaxy subsamples. To select centrals, we implemented the criterion $P_{sat} < 0.1$. To select satellites, we set $P_{sat} > 0.9$. These selections yielded two subsamples with 2217 central and 902 satellite galaxies. Their distribution in M_h and M_* space is shown in Figure 1.

3. METHODOLOGY

3.1. Central and satellite subsamples

This section presents the different subsamples of central and satellite galaxies. The overall distribution of our centrals and satellites in M_* and M_h is plotted in the left panel of Figure 1. To properly compare the samples, we constructed 241 pairs of centrals and satellites that have matching M_* and M_h (top right panel of Figure 1). To characterize how satellite formation depends on M_h , we defined two more satellite subsamples: low- M_h satellites and high- M_h satellites (middle right panel of Figure 1). These subsamples were defined to include only satellites below and above the 50th percentile in M_* -to- M_h ratio as a function of M_* . We note that the difference in M_h between the two satellite subsamples decreases with M_* .

The epoch at which the satellite first crosses the virial radius of the host halo (infall time; T_{inf}) is another property that could shape the stellar populations of satellite galaxies. [Gallazzi et al. \(2020\)](#) selected ancient ($T_{inf} > 5$ Gyr) and recent ($T_{inf} < 2.5$ Gyr) infallers by characterizing how T_{inf} is mapped onto the projected phase space composed of cluster-centric velocity and distance ([Pasquali et al. 2019](#); [Smith et al. 2019](#)). Here, we implement a similar, albeit more simplistic, analysis based on cluster-centric distance only. As in [Pasquali et al. \(2019\)](#) and [Smith et al. \(2019\)](#), we define the projected, normalized cluster-centric distance as

$$D_{proj} = r_{proj}/r_{200} \quad (2)$$

$$r_{200}[\text{kpc h}^{-1}] = 258.1 \times \frac{(M_h/10^{12})^{1/3} \times (\Omega_m/0.25)^{1/3}}{(1+z)},$$

where r_{proj} is the projected distance between the central and satellite, r_{200} is the virial radius ([Yang et al. 2007](#); [Pasquali et al. 2019](#)), $\Omega_m = 0.3$, and $h = 0.7$.

Based on D_{proj} , we defined two more subsamples. inner-orbit satellites have $D_{proj} < 0.3$, and are meant to resemble the ancient infaller selection. According to Table 1 in [Pasquali et al. \(2019\)](#), inner-orbit satellites have an average $\bar{T}_{inf} \sim 5$ Gyr and standard deviation

$\sigma_{inf} \sim 2.5$ Gyr. Based on these numbers, we estimate a recent infaller contamination of 15%.

On the other hand, far-orbit satellites are defined by $D_{proj} > 0.5$ and are similar to recent infallers. Based on Table 1 from [Pasquali et al. \(2019\)](#), far-orbit satellites have $\bar{T}_{inf} \sim 3.5$ Gyr and $\sigma_{inf} \sim 2.5$. We estimate an ancient infaller contamination of around 20%. The subsamples obtained in this cluster-centric distance selection are plotted in the bottom right panel of Figure 1.

Detailed number counts for all subsamples are presented in Table 1. Note that not all satellite galaxies are classified as either inner orbit or far orbit. After defining the subsamples, we computed high signal-to-noise stacked spectra through the process described in the following section.

3.2. Co-addition and stacking of spectra

Within every galaxy, we co-added the spectra into the three annuli $r = [0, 0.5]$, $[0.5, 1]$, and $[1, 1.5]$ effective radii. This step required shifting every spectrum back to the rest frame using the stellar systemic velocity (v_*) maps calculated by the DAP. Then, we stacked the spectra of central and satellite galaxies in each M_* and annular bin. Stacks were obtained by computing the median and errors were quantified through Monte Carlo simulations that accounted for the propagated errors. All spectra were convolved to $\sigma_* = 350 \text{ kms}^{-1}$ and median normalized before stacking. Greater detail on the stacking process can be found in [Oyarzún et al. \(2022\)](#).

3.3. Stellar population fitting with `alf`

The stacked spectra were fitted with the code `alf` to characterize their stellar populations. The program `alf` fits the optical absorption line spectra of old ($\gtrsim 1$ Gyr) stellar systems ([Conroy & van Dokkum 2012](#); [Conroy et al. 2018](#)) to estimate their stellar population parameters. It is based on the MIST isochrones ([Choi et al. 2016](#); [Dotter 2016](#)) and the stellar libraries by [Sánchez-Blázquez et al. \(2006\)](#) and [Villaume et al. \(2017\)](#). Deviations from the solar abundance pattern are quantified in the theoretical response functions ([Conroy et al. 2018](#); [Kurucz 2018](#)).

We fitted for a two-component SFH (i.e. two SSPs), stellar velocity dispersion, IMF, and the abundances of 19 elements. For the IMF, power laws were fit in the ranges 0.08-0.5 M_\odot and 0.5-1 M_\odot , with the IMF slope set to -2.35 for the 1-100 M_\odot range ([Salpeter 1955](#)). We sampled this multivariate posterior with `emcee` ([Foreman-Mackey et al. 2013](#)) using a setup of 1024 walkers, 10^4 burn-in steps, and 100-step chains.

Stellar ages reported throughout correspond to the mass-weighted age of the two-component SFH. Uncer-

⁶ <https://galaxygroupfinder.net>

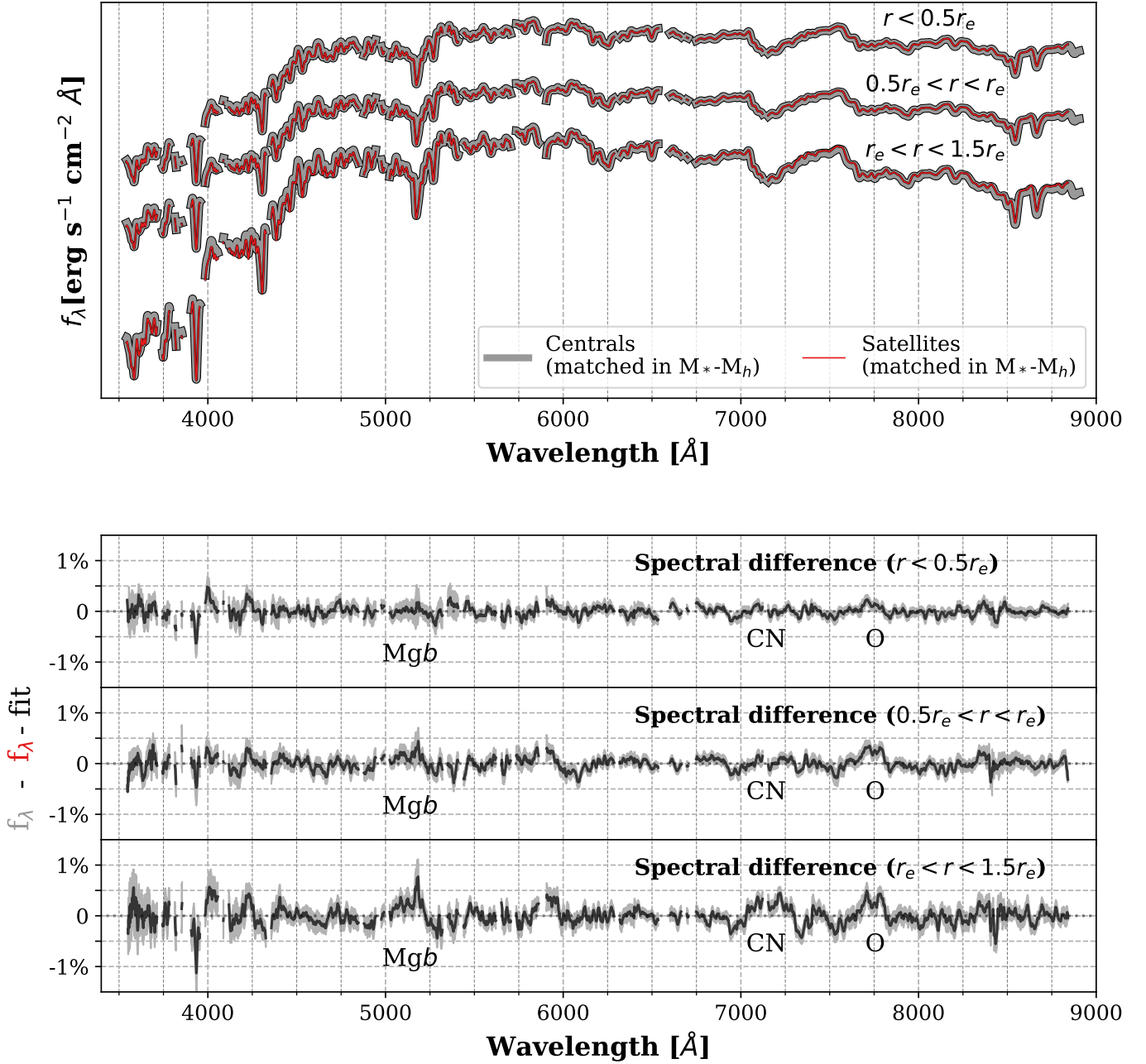


Figure 2. Direct spectral comparison between central and satellite galaxies with matching M_* and M_h . Top: stacked spectra for centrals (gray) and satellites (red) in three radial bins extending from the centers ($r < 0.5r_e$; top) to the outskirts ($r_e < r < 1.5r_e$; bottom). Bottom: spectral difference obtained by subtracting the satellite stack from the central stack in each radial bin. A polynomial was fit to the spectral difference to remove continuum shape variations. Differences are shown in percent relative to the median of the spectrum. The gray shading shows the error on the differences. Centrals and satellites show several significant spectral differences at the 1% level that increase in significance and magnitude as galactocentric distance increases.

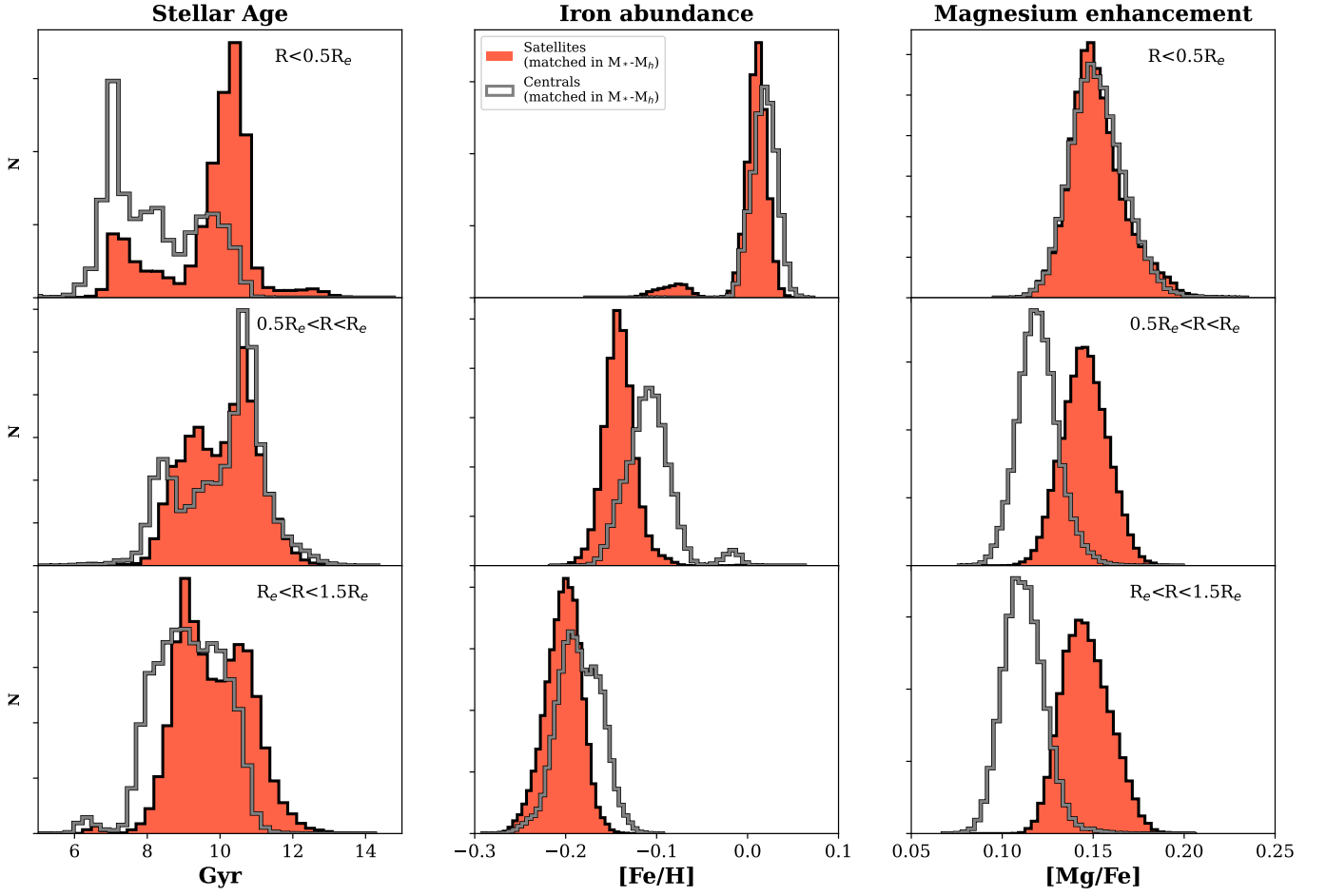


Figure 3. Posterior distributions derived with `alf` for the stellar age, $[\text{Fe}/\text{H}]$, and $[\text{Mg}/\text{Fe}]$ of centrals and satellites with matching M_* and M_h distributions (Figure 2). Central galaxy posteriors are shown in gray, whereas satellite galaxy posteriors are shown in red. Galactocentric distance increases from top to bottom. Satellites are older than centrals in the centers and more Mg-enhanced in the outskirts.

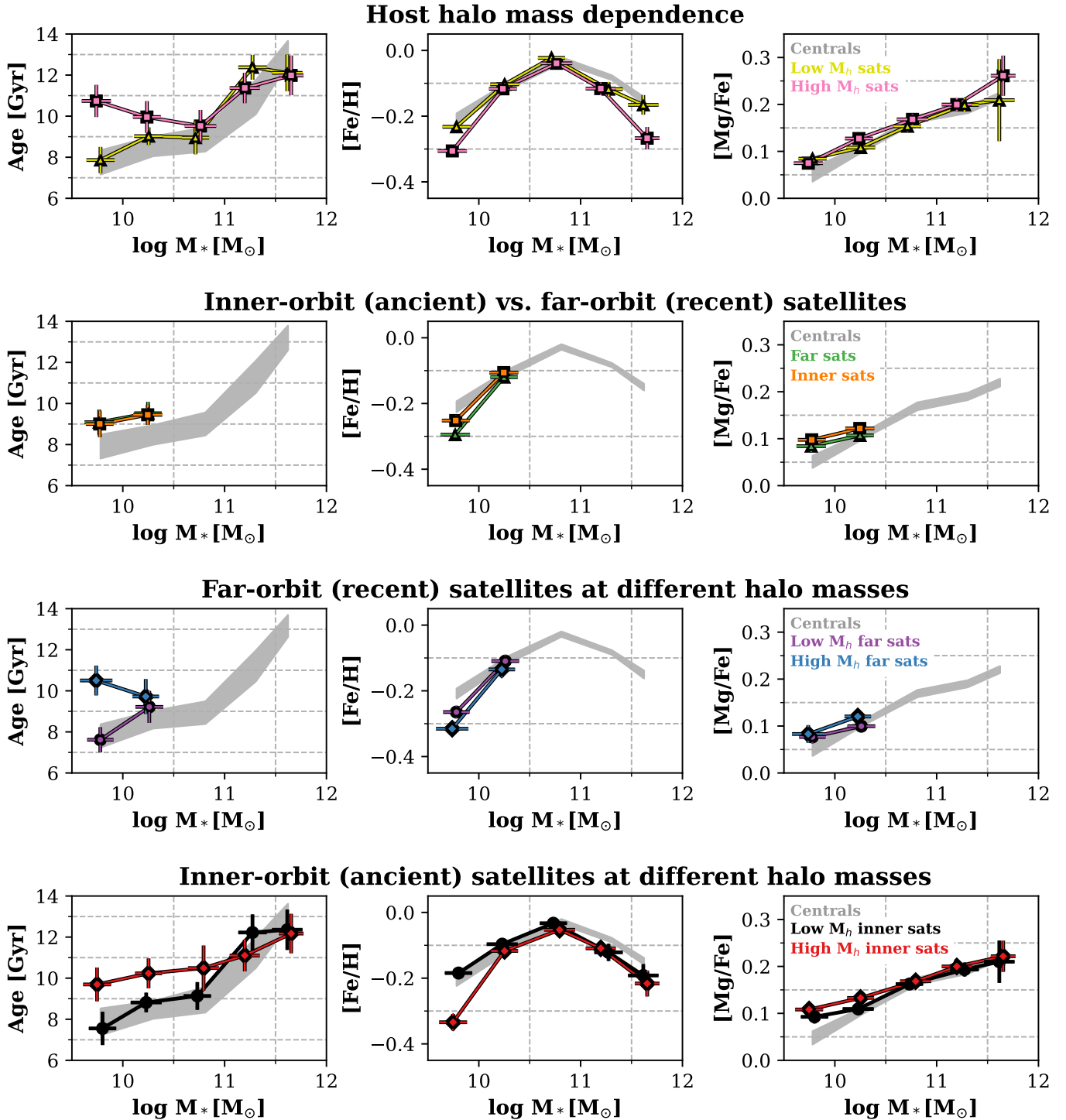


Figure 4. Stellar population parameters integrated within $1.5 r_e$ as a function of M_* . Stellar age is shown on the left, [Fe/H] in the middle, and [Mg/Fe] on the right. Different rows compare centrals against different subsamples of satellite galaxies. In the top two rows, satellites are divided as a function of host halo mass and cluster-centric distance. Both selection methods are combined in the bottom two rows, with far-orbit satellites shown in the third row and inner-orbit satellites at the bottom. For $M_* < 10^{10.5} M_\odot$, satellites found in high- M_h halos are old, have lower [Fe/H], and show higher [Mg/Fe] than centrals, even at fixed cluster-centric distance.

tainties on the fitted parameters account for errors in sample assignment, stacking, and fitting. This was achieved by bootstrapping the selection of galaxies 10 times, and then by stacking and fitting in every iteration.

4. RESULTS

4.1. *Central and satellite galaxies*

Recent works have found that differences between the observable properties of centrals and satellites start to vanish once both M_* and M_h are controlled for (Bluck et al. 2016; Wang et al. 2018b,a,c, 2020). We test whether this conclusion is supported by our data in Figure 2. The top panel shows the stacked spectra for a total of 241 centrals and 241 satellites that have matching M_* and M_h (see Figure 1). It becomes apparent that the stacked spectra of centrals and satellites are very similar in shape and in the strength of their absorption features at all radii.

To identify any spectral variations, we plotted the spectral differences between the stacks as a function of galactocentric distance in the second panel of Figure 2. These spectral differences were computed by subtracting the satellite spectrum from the central spectrum and then fitting polynomials to decouple continuum variations. Despite the subtlety of all spectral differences ($\lesssim 1\%$), some show high significance (e.g. Mgb 5172Å; Faber & Jackson 1976; Faber et al. 1985). There is also clear indication that the magnitude of the spectral differences increases with galactocentric radius.

To translate these differences into stellar population variations, we fitted the stacked spectra with `alf`. We derived posteriors for the mass-weighted stellar age, $[\text{Fe}/\text{H}]$, and $[\text{Mg}/\text{Fe}]$ in three radial bins extending from centers out to $1.5 r_e$ (Figure 3). At the centers, satellites are older than centrals by ~ 2 Gyr. In the outskirts ($r = 0.5\text{-}1.5 r_e$), satellites show higher $[\text{Mg}/\text{Fe}]$ by $\lesssim 0.05$ dex.

4.2. *How the stellar populations of satellites depend on M_h and cluster-centric distance*

We now turn to our analysis of the stellar population parameters of centrals and satellites selected as a function of host M_h and cluster-centric distance (Figure 1). Stacked spectra for galaxies within these subsamples were derived and fitted with `alf`. The recovered stellar population parameters within $1.5 r_e$ as a function of M_* are presented in Figure 4. These radially integrated values were derived via Monte Carlo simulations of radial averaging from the three radially dependent posterior distributions measured with `alf`. The datapoints and error bars shown in Figure 4 therefore correspond to

the median and the standard deviation of the radial-average distributions for every subsample and M_* bin. Instead of running `alf` on spectra stacked out to $1.5 r_e$, our approach ensures that the radial averages are not dependent surface brightness, i.e., all radial scales are weighted equally.

Generally, the ages of central and satellite galaxies increase from ~ 8 Gyr at $M_* = 10^{10} M_\odot$ to > 10 Gyr for $M_* > 10^{11} M_\odot$, in agreement with previous observations that galaxies of increasing M_* are older (e.g. Gallazzi et al. 2005; McDermid et al. 2015; Lacerna et al. 2020). As for $[\text{Fe}/\text{H}]$, its magnitude increases with M_* before turning over around $M_* \sim 10^{11} M_\odot$. This might seem to contradict the stellar mass-metallicity relation, in which metallicity always increases with the M_* or central velocity dispersion of the galaxy (Faber & Jackson 1976; Cid Fernandes et al. 2005; Gallazzi et al. 2005; Thomas et al. 2005, 2010; González Delgado et al. 2014; McDermid et al. 2015). However, stellar metallicity typically refers to a weighted average of the abundance of various elements (i.e., a rescaling of the solar abundance pattern), whereas the $[\text{Fe}/\text{H}]$ that we measured with `alf` maps the abundance of iron only. As we pointed out in Oyarzún et al. (2022), the decrease in $[\text{Fe}/\text{H}]$ with M_* at the massive end is likely a consequence of how the star-formation timescales of galaxies shorten as M_* increases. The abundance of magnesium—a proxy for $[\alpha/\text{Fe}]$ (e.g. Faber & Jackson 1976; Faber et al. 1985; Thomas et al. 2005)—monotonically increases with M_* , supporting this interpretation.

The first row of Figure 4 highlights a comparison between satellites in halos of different masses. Satellites in high- M_h halos are older than counterparts in low- M_h halos by ~ 2 Gyr for $M_* < 10^{10.5} M_\odot$. We also observe slightly lower $[\text{Fe}/\text{H}]$ and higher $[\text{Mg}/\text{Fe}]$ in high- M_h satellites.

To quantify the significance of these subtle stellar population differences, we can turn to a Bayesian model comparison. We will consider two models: in model \mathcal{A} the magnitude of the stellar population parameter \mathcal{X} is greater in high- M_h satellites, whereas in model \mathcal{B} the magnitude of \mathcal{X} is greater in low- M_h satellites. By assuming that the two models account for all possible options (e.g. Oyarzún et al. 2017, 2022), the probabilities

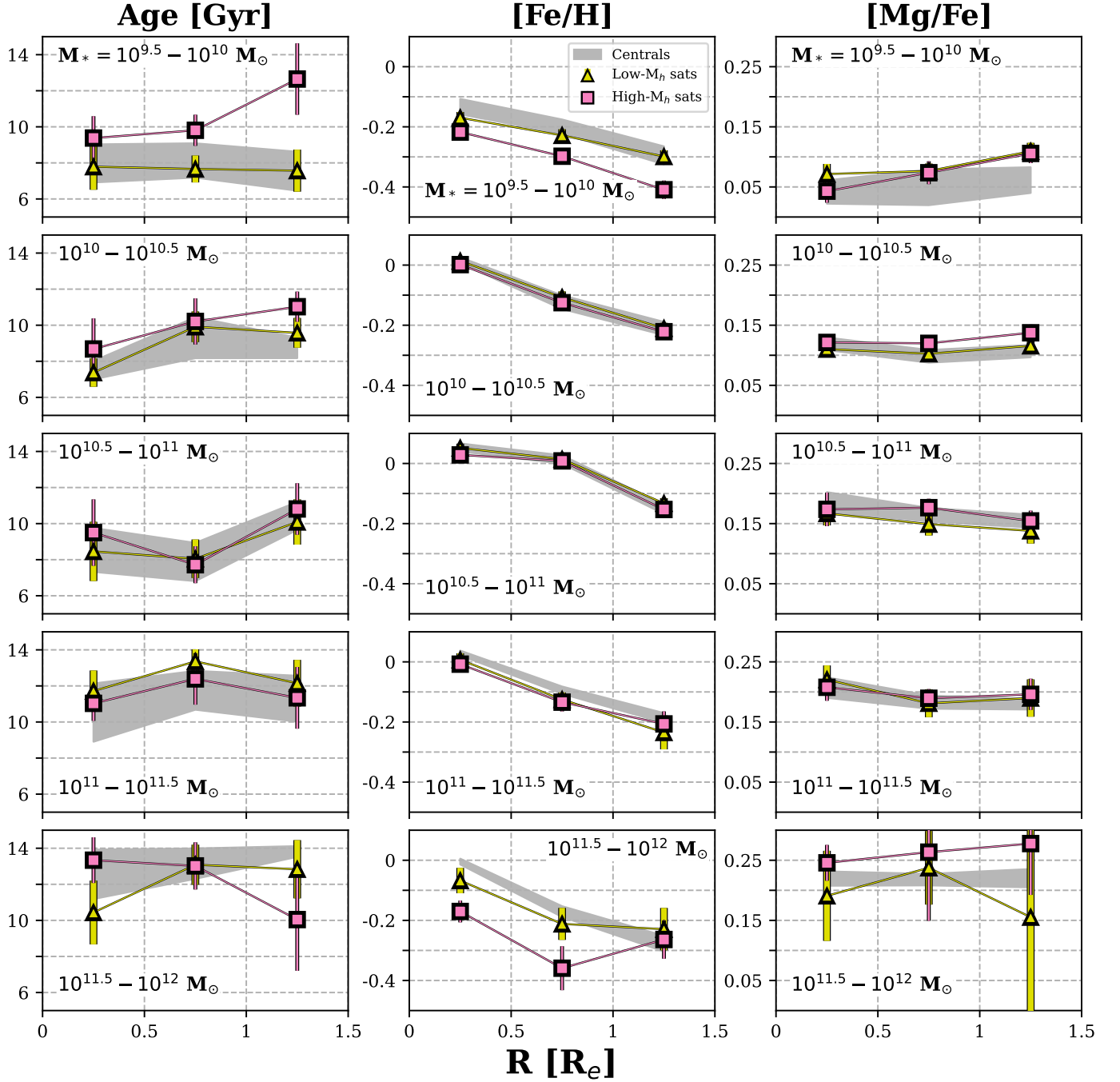


Figure 5. Stellar population profiles of centrals (gray), low- M_h satellites (yellow), and high- M_h satellites (magenta). Stellar mass increases from top to bottom. From left to right, the columns show stellar age, iron abundance, and magnesium enhancement.

of models \mathcal{A} and \mathcal{B} become

$$\text{IP}(\mathcal{A}) = \frac{p_{\mathcal{A}}}{p_{\mathcal{A}} + p_{\mathcal{B}}} \wedge \text{IP}(\mathcal{B}) = \frac{p_{\mathcal{B}}}{p_{\mathcal{A}} + p_{\mathcal{B}}} \quad (3)$$

$$p_{\mathcal{A}} = \prod_{M_*} \text{IP}(\mathcal{X}_{\text{high-}M_h} > \mathcal{X}_{\text{low-}M_h}) \quad (4)$$

$$p_{\mathcal{B}} = \prod_{M_*} \text{IP}(\mathcal{X}_{\text{low-}M_h} < \mathcal{X}_{\text{high-}M_h}) \quad (5)$$

Integrated over the range $M_* = 10^{9.5} - 10^{10.5} M_{\odot}$, high- M_h satellites have older ages, lower $[\text{Fe}/\text{H}]$, and higher $[\text{Mg}/\text{Fe}]$ than low- M_h satellites of the same M_* with 3.2σ , 5.7σ , and 2.4σ significance, respectively. Taken together, these results indicate that satellites found in more massive dark matter halos formed their stars, on average, earlier and in shorter timescales.

The stellar populations of satellite galaxies can also depend on properties other than host M_h . Gallazzi et al. (2020) argued that the old ages of high- M_h satellites can be driven by ancient infallers ($T_{inf} > 5$ Gyr), which are primarily found at small cluster-centric distances. We examine how the satellite stellar populations depend on cluster-centric distance in the second row of Figure 4. Although there is no evidence of stellar age differences with cluster-centric distance, there is some evidence that inner-orbit satellites have higher $[\text{Fe}/\text{H}]$ (2.6σ) and higher $[\text{Mg}/\text{Fe}]$ (1.8σ) than far-orbit satellites.

We also show in Figure 4 that the differences between satellites with varying host M_h are also present when cluster-centric distance is controlled for. As can be seen in the third row of this figure, far-orbit satellites in high- M_h halos feature older ages, lower $[\text{Fe}/\text{H}]$, and higher $[\text{Mg}/\text{Fe}]$ than far-orbit satellites in low- M_h halos, at least for the M_* range probed by our far-orbit satellite subsample (see Figure 1). The direction and magnitude of these differences with host M_h are also seen in the inner-orbit satellite subsample (fourth row).

Central galaxies are plotted with gray shading to provide a rough point of reference. A quantitative comparison between centrals and satellites is not possible in Figure 4, however, because these two samples have not been matched in M_* and M_h (for that comparison, see Figure 3). That said, the differences we detected in Figure 3 are qualitatively apparent in Figure 4, with all satellite subsamples showing higher $[\text{Mg}/\text{Fe}]$ in most M_* bins. In regards to how the stellar populations of centrals vary with M_h at fixed M_* , we showed in Oyarzún et al. (2022) that those variations are small and within the uncertainties shown in Figure 4.

4.3. The stellar population profiles

We can also gain insight into how central and satellite galaxies form through the radial distribution of their stellar populations. The profiles at different M_* are compared in Figure 5. From left to right, shown are stellar age, $[\text{Fe}/\text{H}]$, and $[\text{Mg}/\text{Fe}]$. The stellar age profiles are mostly flat within our error bars for all subsamples, in agreement with other work on the stellar population gradients of massive galaxies (Goddard et al. 2017b,a; Zheng et al. 2017; Lacerna et al. 2020). On the other hand, the $[\text{Fe}/\text{H}]$ profiles fall with galactocentric distance (e.g. Greene et al. 2015; Parikh et al. 2018, 2019). As measured in Parikh et al. (2019), the $[\text{Mg}/\text{Fe}]$ profiles are constant with galactocentric distance in most cases.

We notice systematic offsets in the normalization of satellite profiles with different M_h that mirror the results shown in Figure 4 and described in the previous

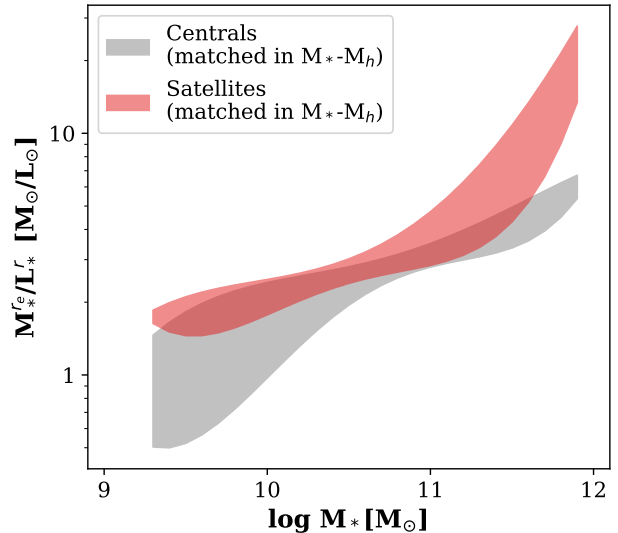


Figure 6. Comparison between the stellar mass-to-light ratios of central and satellite subsamples matched in M_* and M_h (1σ contours). Stellar masses were measured in MaNGA and account for the mass within the r_e only. Galaxy luminosities were measured in r-band photometry from the DESI Legacy Imaging Survey (Dey et al. 2019) as described in Tinker (2020b). Note how centrals have lower M_*^e/L_* , likely as a result of their greater stellar masses beyond the r_e (e.g. Huang et al. 2013a).

section. Figure 5 reveals that variations in the integrated properties of satellites with M_h (Figure 4) are for the most part systematic with galactocentric distance. Regarding variations in the *shape* of the profiles, the increased uncertainties resulting from additional binning in galactocentric distance prevent us from detecting any statistically significant signals.

5. DISCUSSION

We have found that stellar populations in the outskirts of passive satellite galaxies are more alpha enhanced than the stellar populations in the outskirts of passive central galaxies of the same M_* and M_h . We also found that passive satellites in high- M_h halos feature older stellar ages, lower $[\text{Fe}/\text{H}]$, and higher $[\text{Mg}/\text{Fe}]$ than passive satellites in low- M_h halos, especially for $M_* = 10^{9.5} - 10^{10.5} M_\odot$. We now aim to place these results in a physical context and compare them with previous work.

5.1. Inferences from direct spectral comparison

While previous work has found passive satellite galaxies to be older and more alpha enhanced than centrals of the same M_* (e.g. Gallazzi et al. 2020), it has not been possible to control for a possible bias in host M_h (e.g. Wang et al. 2018b, 2020). We know that satellites reside

in more massive halos than centrals at fixed M_* (Figure 1) and that centrals become older and more alpha enhanced as M_h increases (Oyarzún et al. 2022), and thus we might attribute the differences between centrals and satellites to how M_h modulates galaxy formation.

Figure 2 was designed to search for spectral differences between centrals and satellites while controlling for both M_* and M_h . We detected significant spectral differences between central and satellite spectra at the 1% level, which is direct evidence that galaxy formation is not agnostic to whether the galaxy is a central or a satellite. Linking these spectral differences to stellar population variations reveals that satellites are older in the centers and more alpha enhanced in the outskirts than centrals (Figure 3).

Also telling is how the magnitude of these spectral differences increases with galactocentric distance. This could be an indication that the physical processes driving these differences are operating from the outside-in. From a satellite perspective, gas reservoirs in the outskirts may be stripped away by host halo-driven processes like starvation, leading to outside-in quenching (Section 5.2). On the other hand, central galaxies may be growing their outskirts through the accretion of smaller satellite galaxies (Section 5.4). Both scenarios are discussed in detail in the following sections.

5.2. The environment-driven quenching scenario

Through processes like starvation and strangulation, massive halos can strip satellite galaxies of their cold and hot gas reservoirs, suppressing future star-formation (Larson et al. 1980; Kawata & Mulchaey 2008). These mechanisms are believed to act on timescales of 2-6 Gyr, after which the satellite galaxy would rapidly quench within 1 Gyr, and its stellar populations would then appear old and alpha enhanced (*delayed-then-rapid*; Wetzel et al. 2012, 2013; Fossati et al. 2017; Cora et al. 2019). This is indeed what we see in Figure 3, and is further apparent among high- M_h halos shown in Figure 4. More massive halos may be exerting stronger tidal forces and thus more efficiently removing gas from satellite galaxies (Kang & van den Bosch 2008). The suppression of star-formation also prevents the satellite galaxy from recycling metals like Fe that form on long timescales. Central galaxies, on the other hand, can keep forming stars for longer, increasing their [Fe/H] relative to satellites (Figures 3 and 4). As might be expected with longer timescales of star formation, Figure 3 also shows some evidence for younger stellar populations in centrals that have been M_* and M_h matched to satellites.

Using spatially unresolved SDSS observations, Pasquali et al. (2010) and Gallazzi et al. (2020) found

satellite galaxies to show higher stellar metallicities— $\log Z/Z_\odot$ —than centrals of the same M_* . The results in Gallazzi et al. (2020) are particularly relevant to this work because they were not only recovered in the whole galaxy population, but also in their subsample of passive galaxies. However, it is difficult to directly compare these results with our findings given that $\log Z/Z_\odot$ depends on the abundance of iron, magnesium, and other alpha elements, which we have shown to vary in different subsamples. Yet, the fact that $\log Z/Z_\odot$ monotonically increases with M_* has been used to test another environment-driven mechanism: tidal stripping. This mechanism reduces satellite M_* while leaving stellar metallicity unaffected (Kang & van den Bosch 2008). This can cause satellites to show higher metallicities than expected for their M_* (Pasquali 2015). That said, we note that tidal stripping is thought to dominate at masses lower than the mass range of these works ($M_* < 10^8 M_\odot$; Weisz et al. 2015; Davies et al. 2016; Kawinwanichakij et al. 2017).

One implication of environment-driven quenching is that the time of quenching is dependent on the time of infall of the satellite. Starvation and strangulation begin earlier in ancient infallers ($T_{infall} > 5$ Gyr; Pasquali et al. 2019) compared to recent infallers ($T_{infall} < 2.5$ Gyr; Pasquali et al. 2019). Ancient infallers also tend to orbit closer to the halo center (*inner-orbits*), where the external quenching processes are strongest (van de Voort et al. 2017; Cleland & McGee 2021). Indeed, Gallazzi et al. (2020) found ancient infallers to have older ages, higher $\log Z/Z_\odot$, and greater $[\alpha/Fe]$ than recent infallers for $M_* \sim 10^{10} M_\odot$.

However, Gallazzi et al. (2020) did not separate satellite galaxies into star-forming and passive for their time-of-infall analysis. In this paper, we studied passive galaxies only and adopted a cruder definition of *ancient* and *recent* infallers. Our result is shown in the second row of Figure 4. While far more subtle than in Gallazzi et al. (2020), we see some evidence for increased [Fe/H] and [Mg/Fe] among the inner-orbit satellites that we associate with ancient infallers.

Focusing on ancient infallers only, Gallazzi et al. (2020) found their stellar ages and $[\alpha/Fe]$ to correlate with host M_h , in agreement with our Figure 4 (bottom row). Their analysis of recent infallers, on the other hand, yielded little stellar population variations with host M_h . In contrast, other work has found evidence that recent infallers feature lower sSFR and older ages than field galaxies of the same M_* (Pasquali et al. 2019). In addition, Smith et al. (2019) found evidence that clusters impact the star-formation histories of satellite galaxies before they enter the virial radius of the

host halo. Our results from Figure 4 better align with the findings in Pasquali et al. (2019) and Smith et al. (2019), in support of a picture where massive halos can affect the assembly of satellites in far orbits as well.

This notion is often associated with *preprocessing*. Here, satellite cold gas reservoirs are heated up (i.e., evaporation) and/or warm subhalo gas is stripped (i.e. strangulation) by the hot ICM gas (Fujita 2004) even before they enter the virial radius of the host halo (Pallero et al. 2019). This scenario not only can explain the differences with host M_h in the populations of recent infallers, but also subtle variations in the quenched fraction of galaxies at large cluster-centric distances (Haines et al. 2015; Bianconi et al. 2018; van der Burg et al. 2018; Sarron et al. 2019; Sarron & Conselice 2021).

Cosmological simulations also provide support for this scenario. Lacerna et al. (2022) found that quenched central galaxies of $M_* \sim 10^{10} M_\odot$ are, on average, 5 times closer to the nearest massive group or cluster than star-forming centrals of the same M_* . This result not only is consistent with preprocessing, but can also explain the similarity between the properties of galaxies in adjacent halos (i.e., two-halo conformity; Kauffmann et al. 2013; Hearin et al. 2015).

In summary, we have shown that centrals and satellites show differences in their assembly histories that cannot be fully ascribed to M_h variations. Environment-driven quenching provides an explanation for these trends, qualitatively explaining why satellites have older ages, lower [Fe/H], higher [Mg/Fe], and higher quenched fractions (Davies et al. 2019) than centrals, even after controlling for both M_* and M_h . That said, our picture of environment-driven quenching needed to be broadened to include preprocessing effects that occur at very large cluster-centric distances before infalling galaxies enter the halo.

5.3. *Stellar population variations in the outskirts from an environment-driven quenching perspective*

Through processes like gas ram pressure and evaporation, host halos can strip weakly bound neutral gas from the outskirts of satellite galaxies via tidal and hydrodynamical effects, inhibiting the formation of HII in the outer disk (Cortese et al. 2021) and quenching the galaxy from the outside-in (Chung et al. 2009). This has motivated a search for variations in the stellar population parameters of satellites with galactocentric distance, although no conclusive evidence has been found (e.g. Goddard et al. 2017a; Zheng et al. 2017; Santucci et al. 2020; Zhou et al. 2020).

The strongest indication that satellites are subject to unique processes in their outskirts comes from our

direct spectral comparison (Figure 2). Without any stellar population characterization, we detected systematic differences in how central and satellite galaxies assemble their stellar components. These differences are magnified beyond the r_e and are caused by variations in [Mg/Fe] (Figure 3), indicating that satellite galaxies assembled their outskirts over remarkably short timescales.

Other patterns observed in MaNGA and SAMI (Allen et al. 2015) also support an environment-driven, outside-in picture for satellite quenching. The outskirts of star-forming galaxies in high-density regions show evidence of star-formation suppression (Schaefer et al. 2017) and M_* deficit (Spindler & Wake 2017). In contrast, other works have also reported signatures of *inside-out* quenching (Lin et al. 2019), highlighting that further studies of low-mass galaxies are required to better tease out these mechanisms.

5.4. *The stellar accretion scenario*

Group finding algorithms, including the one used in this paper, match groups in luminosity with dark-matter halos in M_h by their abundance (i.e. abundance matching). This means that if a central and satellite are observed to have the same M_* within the r_e ($M_*^{r_e}$) and their respective groups have the same M_h , then their total r-band luminosity (L_*^r) must differ. This is highlighted in Figure 6, where centrals and satellites that have been matched in M_* and M_h follow different tracks in $M_*^{r_e}/L_*^r$.

The lower $M_*^{r_e}/L_*^r$ of central galaxies can be interpreted in the context of their peculiar surface brightness profiles. While the centers of massive central galaxies ($r < 1$ kpc) are very compact, their outskirts feature faint, extended, highly elliptical outer envelopes ($r > 10$ kpc) that presumably assembled through the accretion of stellar envelopes from satellite galaxies (Huang et al. 2013a,b, 2018). This picture suggests that differences between the stellar populations of central and satellite galaxies could be due to differences in their accretion histories.

In principle, we could attribute the deficit of [Mg/Fe] in centrals (Figure 3) to the accretion of either Mg-poor or Fe-enriched stellar envelopes. However, given how minor the differences in [Fe/H] between centrals and satellites are (Figure 3), the element driving the differences in [Mg/Fe] must be magnesium. For stellar accretion to explain the differences between the stellar populations of centrals and satellites, we need these accreted stellar envelopes formed to be Mg-poor.

To test the validity of this picture, we can turn to hydrodynamical simulations. In Illustris (Rodríguez-

Gomez et al. 2016), the characteristic M_* difference between a central galaxy and the accreted satellite is $\Delta \log M_* \sim 0 - 0.5$. Since $[\text{Mg}/\text{Fe}]$ is a monotonically increasing function of M_* (Figure 4), the expectation is that *ex-situ* stellar populations are more Mg-poor than *in-situ* stellar populations. This line of thought is consistent with the deficit of $[\text{Mg}/\text{Fe}]$ in central galaxies from Figure 3.

In the scenario proposed, central galaxies with higher *ex-situ* mass fractions should have, on average, higher alpha abundances. However, we found the exact opposite in our characterization of central galaxy stellar populations: at fixed M_* , central galaxies in more massive dark-matter halos host more alpha enhanced stars (Oyarzún et al. 2022). Taking into account that centrals in massive halos show stronger merger growth signatures (Huang et al. 2020), our result casts doubts over whether the stellar population differences between centrals and satellites could be driven by differences in their accretion histories.

It is interesting to consider how systematic variations between the M_h of centrals and the M_h of satellite subhalos (i.e., the M_h prior to infall) could also produce differences in the enrichment of magnesium. Perhaps the halos of central galaxies can efficiently sustain accretion of pristine gas, keeping them relatively Mg-poor. Satellite galaxies, on the other hand, might have assembled as centrals in environments of particularly high density, limiting their ability to sustain cold flows of gas and keeping them Mg-enriched as a result.

6. SUMMARY

In this work, we took advantage of the sample size and radial coverage of the MaNGA survey to compute high signal-to-noise stacked spectra for central and satellite galaxies out to $1.5 r_e$. By using the stellar population fitting code `alf` and the Tinker (2020b) group catalog, we were able to constrain the stellar age, $[\text{Fe}/\text{H}]$, and $[\text{Mg}/\text{Fe}]$ profiles of centrals and satellite galaxies as a function of M_* , M_h , and cluster-centric distance. We found the following:

(1). At fixed M_* and M_h , central and satellite galaxies show significant spectral differences at the 1% level that grow in magnitude and significance as galactocentric distance increases. We associate these differences with variations in $[\text{Mg}/\text{Fe}]$, with satellite galaxies featuring more alpha enhanced stellar populations. This result reveals that differences between the stellar populations of centrals and satellites of the same M_* cannot be fully ascribed to variations in M_h . We consider two scenarios to explain these spectral differences:

Environment-driven quenching: Satellite quenching is facilitated by gravitational and hydrodynamical interactions with their host halos. Star-formation in the outskirts of satellites is inhibited, leading to *outside-in* quenching signatures in the spatially resolved stellar populations.

Stellar accretion: Central galaxies have built up their outskirts through the accretion of stellar envelopes from satellite galaxies. As a result, the outskirts of centrals contain alpha deficient stellar populations that originally formed in lower M_* satellite galaxies.

(2). The stellar populations of satellite galaxies depend on the mass of the host halo. Satellites in high- M_h halos feature older stellar ages, lower $[\text{Fe}/\text{H}]$, and higher $[\text{Mg}/\text{Fe}]$ than satellites in low- M_h halos. A possible explanation for this result is that massive host halos quench satellite galaxies at earlier times (e.g. Pasquali et al. 2010; Gallazzi et al. 2020). Alternatively, these results could be driven by how the assembly histories of galaxies vary with the local environment (e.g. Oyarzún et al. 2022).

We thank everyone at UC Santa Cruz involved in the installation and maintenance of the supercomputer Graymalkin, which was used to run `alf` on MaNGA spectra. We acknowledge use of the lux supercomputer at UC Santa Cruz, funded by NSF MRI grant AST 1828315. This work made use of GNU Parallel (Tange 2018). G.O. acknowledges support from the Regents' Fellowship from the University of California, Santa Cruz. K.B. was supported by a UC-MEXUS-CONACYT Grant. R.Y. would like to acknowledge support from the Hong Kong Global STEM Scholar scheme, the Direct Grant of CUHK Faculty of Science, and the Research Grant Council of the Hong Kong Special Administrative Region, China (Project No. 14302522). I.L. acknowledges support from Proyecto DIUDA Programa Inserción No. 22414 of Universidad de Atacama. This research made use of Marvin, a core Python package and web framework for MaNGA data, developed by Brian Cherinka, José Sánchez-Gallego, and Brett Andrews. Funding for SDSS-IV has been provided by the Alfred P. Sloan Foundation, the U.S. Department of Energy Office of Science, and the Participating Institutions. SDSS acknowledges support and resources from the Center for High-Performance Computing at the University of Utah. The SDSS website is <https://www.sdss.org>. SDSS is managed by the Astrophysical Research Consortium for the Participating Institutions of the SDSS Collaboration including the Brazilian Participation Group, the Carnegie Institution for Science, Carnegie Mellon University, the Chilean Participation Group, the French Participation Group,

Harvard-Smithsonian Center for Astrophysics, Instituto de Astrofísica de Canarias, The Johns Hopkins University, Kavli Institute for the Physics and Mathematics of the Universe (IPMU)/University of Tokyo, Lawrence Berkeley National Laboratory, Leibniz Institut für Astrophysik Potsdam (AIP), Max-Planck-Institut für Astronomie (MPIA Heidelberg), Max-Planck-Institut für Astrophysik (MPA Garching), Max-Planck-Institut für Extraterrestrische Physik (MPE), National Astronomical Observatories of China, New Mexico State Univer-

sity, New York University, University of Notre Dame, Observatório Nacional/MCTI, The Ohio State University, Pennsylvania State University, Shanghai Astronomical Observatory, United Kingdom Participation Group, Universidad Nacional Autónoma de México, University of Arizona, University of Colorado Boulder, University of Oxford, University of Portsmouth, University of Utah, University of Virginia, University of Washington, University of Wisconsin, Vanderbilt University, and Yale University.

REFERENCES

- Abdurro'uf, Accetta, K., Aerts, C., et al. 2022, *ApJS*, 259, 35, doi: [10.3847/1538-4365/ac4414](https://doi.org/10.3847/1538-4365/ac4414)
- Aguado, D. S., Ahumada, R., Almeida, A., et al. 2019, *ApJS*, 240, 23, doi: [10.3847/1538-4365/aaf651](https://doi.org/10.3847/1538-4365/aaf651)
- Alam, S., Albareti, F. D., Allende Prieto, C., et al. 2015, *ApJS*, 219, 12, doi: [10.1088/0067-0049/219/1/12](https://doi.org/10.1088/0067-0049/219/1/12)
- Allen, J. T., Croom, S. M., Konstantopoulos, I. S., et al. 2015, *MNRAS*, 446, 1567, doi: [10.1093/mnras/stu2057](https://doi.org/10.1093/mnras/stu2057)
- Balogh, M. L., & Morris, S. L. 2000, *MNRAS*, 318, 703, doi: [10.1046/j.1365-8711.2000.03826.x](https://doi.org/10.1046/j.1365-8711.2000.03826.x)
- Belfiore, F., Westfall, K. B., Schaefer, A., et al. 2019, *AJ*, 158, 160, doi: [10.3847/1538-3881/ab3e4e](https://doi.org/10.3847/1538-3881/ab3e4e)
- Bernardi, M., Meert, A., Sheth, R. K., et al. 2013, *MNRAS*, 436, 697, doi: [10.1093/mnras/stt1607](https://doi.org/10.1093/mnras/stt1607)
- Bianconi, M., Smith, G. P., Haines, C. P., et al. 2018, *MNRAS*, 473, L79, doi: [10.1093/mnrasl/slx167](https://doi.org/10.1093/mnrasl/slx167)
- Blanton, M. R., Kazin, E., Muna, D., Weaver, B. A., & Price-Whelan, A. 2011, *AJ*, 142, 31, doi: [10.1088/0004-6256/142/1/31](https://doi.org/10.1088/0004-6256/142/1/31)
- Blanton, M. R., & Roweis, S. 2007, *AJ*, 133, 734, doi: [10.1086/510127](https://doi.org/10.1086/510127)
- Blanton, M. R., Bershad, M. A., Abolfathi, B., et al. 2017, *AJ*, 154, 28, doi: [10.3847/1538-3881/aa7567](https://doi.org/10.3847/1538-3881/aa7567)
- Bluck, A. F. L., Mendel, J. T., Ellison, S. L., et al. 2016, *MNRAS*, 462, 2559, doi: [10.1093/mnras/stw1665](https://doi.org/10.1093/mnras/stw1665)
- Bundy, K., Bershad, M. A., Law, D. R., et al. 2015, *ApJ*, 798, 7, doi: [10.1088/0004-637X/798/1/7](https://doi.org/10.1088/0004-637X/798/1/7)
- Campbell, D., van den Bosch, F. C., Hearin, A., et al. 2015, *MNRAS*, 452, 444, doi: [10.1093/mnras/stv1091](https://doi.org/10.1093/mnras/stv1091)
- Cherinka, B., Andrews, B. H., Sánchez-Gallego, J., et al. 2019, *AJ*, 158, 74, doi: [10.3847/1538-3881/ab2634](https://doi.org/10.3847/1538-3881/ab2634)
- Choi, J., Dotter, A., Conroy, C., et al. 2016, *ApJ*, 823, 102, doi: [10.3847/0004-637X/823/2/102](https://doi.org/10.3847/0004-637X/823/2/102)
- Chung, A., van Gorkom, J. H., Kenney, J. D. P., Crowl, H., & Vollmer, B. 2009, *AJ*, 138, 1741, doi: [10.1088/0004-6256/138/6/1741](https://doi.org/10.1088/0004-6256/138/6/1741)
- Cid Fernandes, R., Mateus, A., Sodré, L., Stasińska, G., & Gomes, J. M. 2005, *MNRAS*, 358, 363, doi: [10.1111/j.1365-2966.2005.08752.x](https://doi.org/10.1111/j.1365-2966.2005.08752.x)
- Cleland, C., & McGee, S. L. 2021, *MNRAS*, 500, 590, doi: [10.1093/mnras/staa3267](https://doi.org/10.1093/mnras/staa3267)
- Conroy, C. 2013, *ARA&A*, 51, 393, doi: [10.1146/annurev-astro-082812-141017](https://doi.org/10.1146/annurev-astro-082812-141017)
- Conroy, C., & Gunn, J. E. 2010, *ApJ*, 712, 833, doi: [10.1088/0004-637X/712/2/833](https://doi.org/10.1088/0004-637X/712/2/833)
- Conroy, C., Gunn, J. E., & White, M. 2009, *ApJ*, 699, 486, doi: [10.1088/0004-637X/699/1/486](https://doi.org/10.1088/0004-637X/699/1/486)
- Conroy, C., & van Dokkum, P. 2012, *ApJ*, 747, 69, doi: [10.1088/0004-637X/747/1/69](https://doi.org/10.1088/0004-637X/747/1/69)
- Conroy, C., Villaume, A., van Dokkum, P. G., & Lind, K. 2018, *ApJ*, 854, 139, doi: [10.3847/1538-4357/aaab49](https://doi.org/10.3847/1538-4357/aaab49)
- Cook, B. A., Conroy, C., Pillepich, A., Rodriguez-Gomez, V., & Hernquist, L. 2016, *ApJ*, 833, 158, doi: [10.3847/1538-4357/833/2/158](https://doi.org/10.3847/1538-4357/833/2/158)
- Cora, S. A., Hough, T., Vega-Martínez, C. A., & Orsi, Á. A. 2019, *MNRAS*, 483, 1686, doi: [10.1093/mnras/sty3214](https://doi.org/10.1093/mnras/sty3214)
- Cortese, L., Catinella, B., & Smith, R. 2021, *PASA*, 38, e035, doi: [10.1017/pasa.2021.18](https://doi.org/10.1017/pasa.2021.18)
- Davies, L. J. M., Robotham, A. S. G., Driver, S. P., et al. 2016, *MNRAS*, 455, 4013, doi: [10.1093/mnras/stv2573](https://doi.org/10.1093/mnras/stv2573)
- Davies, L. J. M., Robotham, A. S. G., Lagos, C. d. P., et al. 2019, *MNRAS*, 483, 5444, doi: [10.1093/mnras/sty3393](https://doi.org/10.1093/mnras/sty3393)
- Davis, M., Efstathiou, G., Frenk, C. S., & White, S. D. M. 1985, *ApJ*, 292, 371, doi: [10.1086/163168](https://doi.org/10.1086/163168)
- Dey, A., Schlegel, D. J., Lang, D., et al. 2019, *AJ*, 157, 168, doi: [10.3847/1538-3881/ab089d](https://doi.org/10.3847/1538-3881/ab089d)
- Dotter, A. 2016, *ApJS*, 222, 8, doi: [10.3847/0067-0049/222/1/8](https://doi.org/10.3847/0067-0049/222/1/8)
- Drory, N., MacDonald, N., Bershad, M. A., et al. 2015, *AJ*, 149, 77, doi: [10.1088/0004-6256/149/2/77](https://doi.org/10.1088/0004-6256/149/2/77)
- Einasto, J., Saar, E., Kaasik, A., & Chernin, A. D. 1974, *Nature*, 252, 111, doi: [10.1038/252111a0](https://doi.org/10.1038/252111a0)

- Faber, S. M., Friel, E. D., Burstein, D., & Gaskell, C. M. 1985, *ApJS*, 57, 711, doi: [10.1086/191024](https://doi.org/10.1086/191024)
- Faber, S. M., & Jackson, R. E. 1976, *ApJ*, 204, 668, doi: [10.1086/154215](https://doi.org/10.1086/154215)
- Fillingham, S. P., Cooper, M. C., Wheeler, C., et al. 2015, *MNRAS*, 454, 2039, doi: [10.1093/mnras/stv2058](https://doi.org/10.1093/mnras/stv2058)
- Foreman-Mackey, D., Hogg, D. W., Lang, D., & Goodman, J. 2013, *PASP*, 125, 306, doi: [10.1086/670067](https://doi.org/10.1086/670067)
- Fossati, M., Wilman, D. J., Mendel, J. T., et al. 2017, *ApJ*, 835, 153, doi: [10.3847/1538-4357/835/2/153](https://doi.org/10.3847/1538-4357/835/2/153)
- Fujita, Y. 2004, *PASJ*, 56, 29, doi: [10.1093/pasj/56.1.29](https://doi.org/10.1093/pasj/56.1.29)
- Gallazzi, A., Charlot, S., Brinchmann, J., White, S. D. M., & Tremonti, C. A. 2005, *MNRAS*, 362, 41, doi: [10.1111/j.1365-2966.2005.09321.x](https://doi.org/10.1111/j.1365-2966.2005.09321.x)
- Gallazzi, A. R., Pasquali, A., Zibetti, S., & La Barbera, F. 2020, arXiv e-prints, arXiv:2010.04733. <https://arxiv.org/abs/2010.04733>
- García-Benito, R., González Delgado, R. M., Pérez, E., et al. 2017, *A&A*, 608, A27, doi: [10.1051/0004-6361/201731357](https://doi.org/10.1051/0004-6361/201731357)
- Goddard, D., Thomas, D., Maraston, C., et al. 2017a, *MNRAS*, 465, 688, doi: [10.1093/mnras/stw2719](https://doi.org/10.1093/mnras/stw2719)
- . 2017b, *MNRAS*, 466, 4731, doi: [10.1093/mnras/stw3371](https://doi.org/10.1093/mnras/stw3371)
- González Delgado, R. M., Cid Fernandes, R., García-Benito, R., et al. 2014, *ApJL*, 791, L16, doi: [10.1088/2041-8205/791/1/L16](https://doi.org/10.1088/2041-8205/791/1/L16)
- Greene, J. E., Janish, R., Ma, C.-P., et al. 2015, *ApJ*, 807, 11, doi: [10.1088/0004-637X/807/1/11](https://doi.org/10.1088/0004-637X/807/1/11)
- Greene, J. E., Veale, M., Ma, C.-P., et al. 2019, *ApJ*, 874, 66, doi: [10.3847/1538-4357/ab01e3](https://doi.org/10.3847/1538-4357/ab01e3)
- Gunn, J. E., & Gott, J. Richard, I. 1972, *ApJ*, 176, 1, doi: [10.1086/151605](https://doi.org/10.1086/151605)
- Gunn, J. E., Siegmund, W. A., Mannery, E. J., et al. 2006, *AJ*, 131, 2332, doi: [10.1086/500975](https://doi.org/10.1086/500975)
- Haines, C. P., Pereira, M. J., Smith, G. P., et al. 2015, *ApJ*, 806, 101, doi: [10.1088/0004-637X/806/1/101](https://doi.org/10.1088/0004-637X/806/1/101)
- Hearin, A. P., Watson, D. F., & van den Bosch, F. C. 2015, *MNRAS*, 452, 1958, doi: [10.1093/mnras/stv1358](https://doi.org/10.1093/mnras/stv1358)
- Huang, S., Ho, L. C., Peng, C. Y., Li, Z.-Y., & Barth, A. J. 2013a, *ApJ*, 766, 47, doi: [10.1088/0004-637X/766/1/47](https://doi.org/10.1088/0004-637X/766/1/47)
- . 2013b, *ApJL*, 768, L28, doi: [10.1088/2041-8205/768/2/L28](https://doi.org/10.1088/2041-8205/768/2/L28)
- Huang, S., Leauthaud, A., Greene, J. E., et al. 2018, *MNRAS*, 475, 3348, doi: [10.1093/mnras/stx3200](https://doi.org/10.1093/mnras/stx3200)
- Huang, S., Leauthaud, A., Hearin, A., et al. 2020, *MNRAS*, 492, 3685, doi: [10.1093/mnras/stz3314](https://doi.org/10.1093/mnras/stz3314)
- Johansson, P. H., Naab, T., & Ostriker, J. P. 2012, *ApJ*, 754, 115, doi: [10.1088/0004-637X/754/2/115](https://doi.org/10.1088/0004-637X/754/2/115)
- Kang, X., & van den Bosch, F. C. 2008, *ApJL*, 676, L101, doi: [10.1086/587620](https://doi.org/10.1086/587620)
- Kauffmann, G., Li, C., Zhang, W., & Weinmann, S. 2013, *MNRAS*, 430, 1447, doi: [10.1093/mnras/stt007](https://doi.org/10.1093/mnras/stt007)
- Kawata, D., & Mulchaey, J. S. 2008, *ApJL*, 672, L103, doi: [10.1086/526544](https://doi.org/10.1086/526544)
- Kawinwanichakij, L., Papovich, C., Quadri, R. F., et al. 2017, *ApJ*, 847, 134, doi: [10.3847/1538-4357/aa8b75](https://doi.org/10.3847/1538-4357/aa8b75)
- Kroupa, P. 2001, *MNRAS*, 322, 231, doi: [10.1046/j.1365-8711.2001.04022.x](https://doi.org/10.1046/j.1365-8711.2001.04022.x)
- Kurucz, R. L. 2018, in *Astronomical Society of the Pacific Conference Series*, Vol. 515, Workshop on Astrophysical Opacities, 47
- La Barbera, F., Pasquali, A., Ferreras, I., et al. 2014, *MNRAS*, 445, 1977, doi: [10.1093/mnras/stu1626](https://doi.org/10.1093/mnras/stu1626)
- Lacerna, I., Ibarra-Medel, H., Avila-Reese, V., et al. 2020, *A&A*, 644, A117, doi: [10.1051/0004-6361/202037503](https://doi.org/10.1051/0004-6361/202037503)
- Lacerna, I., Rodriguez, F., Montero-Dorta, A. D., et al. 2022, *MNRAS*, 513, 2271, doi: [10.1093/mnras/stac1020](https://doi.org/10.1093/mnras/stac1020)
- Larson, R. B., Tinsley, B. M., & Caldwell, C. N. 1980, *ApJ*, 237, 692, doi: [10.1086/157917](https://doi.org/10.1086/157917)
- Law, D. R., Yan, R., Bershady, M. A., et al. 2015, *AJ*, 150, 19, doi: [10.1088/0004-6256/150/1/19](https://doi.org/10.1088/0004-6256/150/1/19)
- Law, D. R., Cherinka, B., Yan, R., et al. 2016, *AJ*, 152, 83, doi: [10.3847/0004-6256/152/4/83](https://doi.org/10.3847/0004-6256/152/4/83)
- Leja, J., Carnall, A. C., Johnson, B. D., Conroy, C., & Speagle, J. S. 2019, *ApJ*, 876, 3, doi: [10.3847/1538-4357/ab133c](https://doi.org/10.3847/1538-4357/ab133c)
- Leja, J., Johnson, B. D., Conroy, C., van Dokkum, P. G., & Byler, N. 2017, *ApJ*, 837, 170, doi: [10.3847/1538-4357/aa5ffe](https://doi.org/10.3847/1538-4357/aa5ffe)
- Lin, L., Hsieh, B.-C., Pan, H.-A., et al. 2019, *ApJ*, 872, 50, doi: [10.3847/1538-4357/aafa84](https://doi.org/10.3847/1538-4357/aafa84)
- Mayer, L., Governato, F., Colpi, M., et al. 2001, *ApJ*, 559, 754, doi: [10.1086/322356](https://doi.org/10.1086/322356)
- Mayer, L., Mastropietro, C., Wadsley, J., Stadel, J., & Moore, B. 2006, *MNRAS*, 369, 1021, doi: [10.1111/j.1365-2966.2006.10403.x](https://doi.org/10.1111/j.1365-2966.2006.10403.x)
- McDermid, R. M., Alatalo, K., Blitz, L., et al. 2015, *MNRAS*, 448, 3484, doi: [10.1093/mnras/stv105](https://doi.org/10.1093/mnras/stv105)
- Moustakas, J., Kennicutt, Robert C., J., & Tremonti, C. A. 2006, *ApJ*, 642, 775, doi: [10.1086/500964](https://doi.org/10.1086/500964)
- Nulsen, P. E. J. 1982, *MNRAS*, 198, 1007, doi: [10.1093/mnras/198.4.1007](https://doi.org/10.1093/mnras/198.4.1007)
- Oke, J. B., & Gunn, J. E. 1983, *ApJ*, 266, 713, doi: [10.1086/160817](https://doi.org/10.1086/160817)
- Oser, L., Naab, T., Ostriker, J. P., & Johansson, P. H. 2012, *ApJ*, 744, 63, doi: [10.1088/0004-637X/744/1/63](https://doi.org/10.1088/0004-637X/744/1/63)
- Oser, L., Ostriker, J. P., Naab, T., Johansson, P. H., & Burkert, A. 2010, *ApJ*, 725, 2312, doi: [10.1088/0004-637X/725/2/2312](https://doi.org/10.1088/0004-637X/725/2/2312)

- Oyarzún, G. A., Blanc, G. A., González, V., Mateo, M., & Bailey, John I., I. 2017, *ApJ*, 843, 133, doi: [10.3847/1538-4357/aa7552](https://doi.org/10.3847/1538-4357/aa7552)
- Oyarzún, G. A., Bundy, K., Westfall, K. B., et al. 2019, *ApJ*, 880, 111, doi: [10.3847/1538-4357/ab297c](https://doi.org/10.3847/1538-4357/ab297c)
- . 2022, *ApJ*, 933, 88, doi: [10.3847/1538-4357/ac7048](https://doi.org/10.3847/1538-4357/ac7048)
- Pallero, D., Gómez, F. A., Padilla, N. D., et al. 2019, *MNRAS*, 488, 847, doi: [10.1093/mnras/stz1745](https://doi.org/10.1093/mnras/stz1745)
- Parikh, T., Thomas, D., Maraston, C., et al. 2018, *MNRAS*, 477, 3954, doi: [10.1093/mnras/sty785](https://doi.org/10.1093/mnras/sty785)
- . 2019, *MNRAS*, 483, 3420, doi: [10.1093/mnras/sty3339](https://doi.org/10.1093/mnras/sty3339)
- Pasquali, A. 2015, *Astronomische Nachrichten*, 336, 505, doi: [10.1002/asna.201512188](https://doi.org/10.1002/asna.201512188)
- Pasquali, A., Gallazzi, A., Fontanot, F., et al. 2010, *MNRAS*, 407, 937, doi: [10.1111/j.1365-2966.2010.17074.x](https://doi.org/10.1111/j.1365-2966.2010.17074.x)
- Pasquali, A., Smith, R., Gallazzi, A., et al. 2019, *MNRAS*, 484, 1702, doi: [10.1093/mnras/sty3530](https://doi.org/10.1093/mnras/sty3530)
- Read, J. I., Wilkinson, M. I., Evans, N. W., Gilmore, G., & Kleyna, J. T. 2006, *MNRAS*, 366, 429, doi: [10.1111/j.1365-2966.2005.09861.x](https://doi.org/10.1111/j.1365-2966.2005.09861.x)
- Rodriguez-Gomez, V., Pillepich, A., Sales, L. V., et al. 2016, *MNRAS*, 458, 2371, doi: [10.1093/mnras/stw456](https://doi.org/10.1093/mnras/stw456)
- Salpeter, E. E. 1955, *ApJ*, 121, 161, doi: [10.1086/145971](https://doi.org/10.1086/145971)
- Sánchez, S. F., Pérez, E., Sánchez-Blázquez, P., et al. 2016a, *RMxAA*, 52, 21. <https://arxiv.org/abs/1509.08552>
- . 2016b, *RMxAA*, 52, 171. <https://arxiv.org/abs/1602.01830>
- Sánchez, S. F., Barrera-Ballesteros, J. K., Lacerda, E., et al. 2022, arXiv e-prints, arXiv:2206.07062. <https://arxiv.org/abs/2206.07062>
- Sánchez-Blázquez, P., Peletier, R. F., Jiménez-Vicente, J., et al. 2006, *MNRAS*, 371, 703, doi: [10.1111/j.1365-2966.2006.10699.x](https://doi.org/10.1111/j.1365-2966.2006.10699.x)
- Santucci, G., Brough, S., Scott, N., et al. 2020, arXiv e-prints, arXiv:2005.00541. <https://arxiv.org/abs/2005.00541>
- Sarron, F., Adami, C., Durret, F., & Laigle, C. 2019, *A&A*, 632, A49, doi: [10.1051/0004-6361/201935394](https://doi.org/10.1051/0004-6361/201935394)
- Sarron, F., & Conselice, C. J. 2021, *MNRAS*, 506, 2136, doi: [10.1093/mnras/stab1844](https://doi.org/10.1093/mnras/stab1844)
- Schaefer, A. L., Croom, S. M., Allen, J. T., et al. 2017, *MNRAS*, 464, 121, doi: [10.1093/mnras/stw2289](https://doi.org/10.1093/mnras/stw2289)
- Smee, S. A., Gunn, J. E., Uomoto, A., et al. 2013, *AJ*, 146, 32, doi: [10.1088/0004-6256/146/2/32](https://doi.org/10.1088/0004-6256/146/2/32)
- Smith, R., Pacifici, C., Pasquali, A., & Calderón-Castillo, P. 2019, *ApJ*, 876, 145, doi: [10.3847/1538-4357/ab1917](https://doi.org/10.3847/1538-4357/ab1917)
- Spindler, A., & Wake, D. 2017, *MNRAS*, 468, 333, doi: [10.1093/mnras/stx427](https://doi.org/10.1093/mnras/stx427)
- Tange, O. 2018, GNU Parallel 2018 (Ole Tange), doi: [10.5281/zenodo.1146014](https://doi.org/10.5281/zenodo.1146014)
- Taylor, P., & Kobayashi, C. 2017, *MNRAS*, 471, 3856, doi: [10.1093/mnras/stx1860](https://doi.org/10.1093/mnras/stx1860)
- Thomas, D., Maraston, C., Bender, R., & Mendes de Oliveira, C. 2005, *ApJ*, 621, 673, doi: [10.1086/426932](https://doi.org/10.1086/426932)
- Thomas, D., Maraston, C., Schawinski, K., Sarzi, M., & Silk, J. 2010, *MNRAS*, 404, 1775, doi: [10.1111/j.1365-2966.2010.16427.x](https://doi.org/10.1111/j.1365-2966.2010.16427.x)
- Tinker, J. L. 2020a, arXiv e-prints, arXiv:2007.12200. <https://arxiv.org/abs/2007.12200>
- . 2020b, arXiv e-prints, arXiv:2010.02946. <https://arxiv.org/abs/2010.02946>
- Trussler, J., Maiolino, R., Maraston, C., et al. 2021, *MNRAS*, 500, 4469, doi: [10.1093/mnras/staa3545](https://doi.org/10.1093/mnras/staa3545)
- van de Voort, F., Bahé, Y. M., Bower, R. G., et al. 2017, *MNRAS*, 466, 3460, doi: [10.1093/mnras/stw3356](https://doi.org/10.1093/mnras/stw3356)
- van den Bosch, F. C., Aquino, D., Yang, X., et al. 2008a, *MNRAS*, 387, 79, doi: [10.1111/j.1365-2966.2008.13230.x](https://doi.org/10.1111/j.1365-2966.2008.13230.x)
- van den Bosch, F. C., Pasquali, A., Yang, X., et al. 2008b, arXiv e-prints, arXiv:0805.0002. <https://arxiv.org/abs/0805.0002>
- van der Burg, R. F. J., McGee, S., Aussel, H., et al. 2018, *A&A*, 618, A140, doi: [10.1051/0004-6361/201833572](https://doi.org/10.1051/0004-6361/201833572)
- Villaume, A., Conroy, C., Johnson, B., et al. 2017, *ApJS*, 230, 23, doi: [10.3847/1538-4365/aa72ed](https://doi.org/10.3847/1538-4365/aa72ed)
- Wake, D. A., Bundy, K., Diamond-Stanic, A. M., et al. 2017, *AJ*, 154, 86, doi: [10.3847/1538-3881/aa7ecc](https://doi.org/10.3847/1538-3881/aa7ecc)
- Wang, E., Wang, H., Mo, H., et al. 2018a, *ApJ*, 864, 51, doi: [10.3847/1538-4357/aad554](https://doi.org/10.3847/1538-4357/aad554)
- Wang, E., Wang, H., Mo, H., van den Bosch, F. C., & Yang, X. 2020, *ApJ*, 889, 37, doi: [10.3847/1538-4357/ab6217](https://doi.org/10.3847/1538-4357/ab6217)
- Wang, E., Wang, H., Mo, H., et al. 2018b, *ApJ*, 860, 102, doi: [10.3847/1538-4357/aac4a5](https://doi.org/10.3847/1538-4357/aac4a5)
- Wang, H., Mo, H. J., Chen, S., et al. 2018c, *ApJ*, 852, 31, doi: [10.3847/1538-4357/aa9e01](https://doi.org/10.3847/1538-4357/aa9e01)
- Wechsler, R. H., & Tinker, J. L. 2018, *ARA&A*, 56, 435, doi: [10.1146/annurev-astro-081817-051756](https://doi.org/10.1146/annurev-astro-081817-051756)
- Weisz, D. R., Dolphin, A. E., Skillman, E. D., et al. 2015, *ApJ*, 804, 136, doi: [10.1088/0004-637X/804/2/136](https://doi.org/10.1088/0004-637X/804/2/136)
- Westfall, K. B., Cappellari, M., Bershady, M. A., et al. 2019, *AJ*, 158, 231, doi: [10.3847/1538-3881/ab44a2](https://doi.org/10.3847/1538-3881/ab44a2)
- Wetzell, A. R., Tinker, J. L., & Conroy, C. 2012, *MNRAS*, 424, 232, doi: [10.1111/j.1365-2966.2012.21188.x](https://doi.org/10.1111/j.1365-2966.2012.21188.x)
- Wetzell, A. R., Tinker, J. L., Conroy, C., & van den Bosch, F. C. 2013, *MNRAS*, 432, 336, doi: [10.1093/mnras/stt469](https://doi.org/10.1093/mnras/stt469)
- White, S. D. M., & Rees, M. J. 1978, *MNRAS*, 183, 341, doi: [10.1093/mnras/183.3.341](https://doi.org/10.1093/mnras/183.3.341)
- Yan, R., Bundy, K., Law, D. R., et al. 2016a, *AJ*, 152, 197, doi: [10.3847/0004-6256/152/6/197](https://doi.org/10.3847/0004-6256/152/6/197)
- Yan, R., Tremonti, C., Bershady, M. A., et al. 2016b, *AJ*, 151, 8, doi: [10.3847/0004-6256/151/1/8](https://doi.org/10.3847/0004-6256/151/1/8)

Yang, X., Mo, H. J., van den Bosch, F. C., et al. 2007, ApJ, 671, 153, doi: [10.1086/522027](https://doi.org/10.1086/522027)

York, D. G., Adelman, J., Anderson, Jr., J. E., et al. 2000, AJ, 120, 1579, doi: [10.1086/301513](https://doi.org/10.1086/301513)

Zheng, Z., Wang, H., Ge, J., et al. 2017, MNRAS, 465, 4572, doi: [10.1093/mnras/stw3030](https://doi.org/10.1093/mnras/stw3030)

Zhou, S., Mo, H. J., Li, C., Boquien, M., & Rossi, G. 2020, MNRAS, 497, 4753, doi: [10.1093/mnras/staa2337](https://doi.org/10.1093/mnras/staa2337)

Zibetti, S., White, S. D. M., Schneider, D. P., & Brinkmann, J. 2005, MNRAS, 358, 949, doi: [10.1111/j.1365-2966.2005.08817.x](https://doi.org/10.1111/j.1365-2966.2005.08817.x)